EPJ B
Condensed Matter and Complex Systems
EPJ.org your physics journal

Eur. Phys. J. B (2019) 92: 264 DOI: 10.1140/epjb/e2019-100377-5

Thermal illusion with the concept of equivalent thermal dipole

Liujun Xu, Shuai Yang, and Jiping Huang

edp sciences
Società Italiana di Fisica
Springer

Eur. Phys. J. B (2019) 92: 264
https://doi.org/10.1140/epjb/e2019-100377-5

THE EUROPEAN PHYSICAL JOURNAL B

Regular Article

Thermal illusion with the concept of equivalent thermal dipole

Liujun Xu[a], Shuai Yang, and Jiping Huang[b]

Department of Physics, State Key Laboratory of Surface Physics, and Key Laboratory of Micro and Nano Photonic Structures (MOE), Fudan University, Shanghai 200438, P.R. China

Received 31 July 2019 / Received in final form 26 October 2019
Published online 2 December 2019

Abstract. The research on thermal illusion contributes to both fundamental theories and practical applications. In the existing literatures, the most common mechanism is to design a shell to disguise the inside core. However, the core-shell scheme may be weak to handle many-particle systems because N particles may require N specially-designed shells. This lacks efficiency and restricts practical applications. To solve this problem, we can no longer focus on the local effect of a single particle. In contrast, we should study the macroscopic effect of the N particles by treating each particle as an equivalent thermal dipole. Then, thermal illusion can be achieved when the macroscopic equivalent thermal dipole moments of different systems are equal to each other. This requires only once calculation and contributes to efficiency. Accidentally, the concept of equivalent thermal dipole helps to revisit the well-known Bruggeman theory and provides a clear physical image for it. The proposed scheme is verified by theoretical analyses, finite-element simulations, and laboratory experiments. Our work offers an efficient approach to achieving thermal illusion in many-particle systems, and contributes to potential applications in misleading infrared detection, manipulating heat flux, etc.

1 Introduction

The past decade has witnessed the development of thermal management with novel thermal metamaterials, such as thermal cloaks [1–9], thermal concentrators [10–15], thermal guiders [16–18], thermal "golden touch" [19], chameleonlike metashells [20]. Recently, thermal illusion [21–28] has attracted intensive research interest for its wide applications. The related scheme is mostly based on the core-shell structure, namely designing a specific shell to disguise the inside core. Although the core-shell scheme is excellent to handle single-particle problems, it seems weak to handle many-particle problems. That is, if N particles should be disguised, N times of calculations may be required to design N specific shells. It is inefficient and inflexible.

To solve this problem, we cannot be restricted to the core-shell scheme, and focus on only the local effect of a single particle. In contrast, we should pay attention to the macroscopic effect of the N particles. Since thermal conductivities can't be directly added or subtracted, a following problem is how to handle the macroscopic effect of the N particles. Inspired by electrostatics, we can treat a thermal particle as an equivalent thermal dipole [29–34]. Concretely speaking, the authors of reference [29] defined the thermal dipole moment, and the authors of references [29–34] used the definition to explore the effective thermal conductivity and mutual interaction of aligned spheroids and graded nanolayers. In this work, we fully discuss the relation between a thermal particle and a thermal dipole, even considering material anisotropy and geometry anisotropy of the thermal particles. In this way, thermal conductivities are vectorized to equivalent thermal dipole moments which possess additivity. Therefore, thermal illusion can be achieved with the concept of equivalent thermal dipole, namely considering the macroscopic equivalent thermal dipole moment of the N particles. It requires only once calculation and contributes to efficiency.

Accidentally, the concept of equivalent thermal dipole helps to draw a clear physical image for the famous Bruggeman theory [35]. Although it has been a long time since the Bruggeman theory was established, the application ranges are still ambiguous [35,36]. We will explain it clearly after the theoretical analyses. In what follows, the scheme is validated by theoretical analyses, finite-element simulations, and laboratory experiments.

2 Theoretical analyses

First, we recall the electrostatic equation $\boldsymbol{\nabla}\cdot(-\varepsilon\boldsymbol{\nabla}\varphi)=\rho_e$ in two dimensions, where ε, φ, and ρ_e are permittivity, electric potential, and charge density, respectively. In the presence of a uniform electric field along the horizontal

[a] e-mail: 13307110076@fudan.edu.cn
[b] e-mail: jphuang@fudan.edu.cn

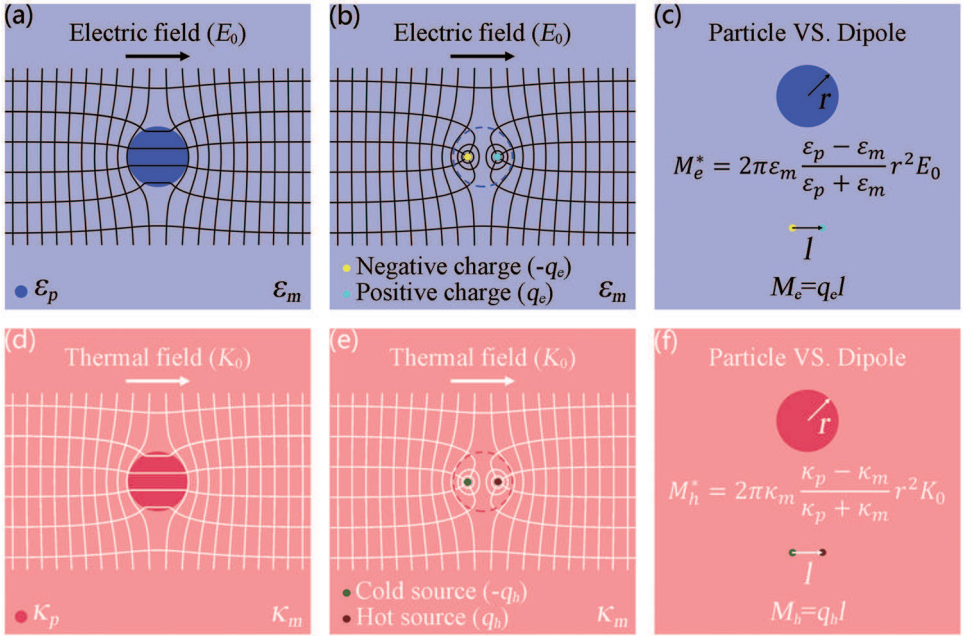

Fig. 1. Two-dimensional counterpart between (a–c) electric field and (d–f) thermal field. (a, b) Present the electric responses of a dielectric particle and an electric dipole in the presence of a uniform electric field E_0, respectively. (c) Shows the mathematical form for treating a dielectric particle as an equivalent electric dipole. (d–f) The thermal counterpart of (a–c).

direction (E_0), a dielectric particle (with permittivity ε_p and radius r) can exert the same effect as an electric dipole (with positive charge q_e and distance l); see Figures 1a and 1b. Compared with the definition of an electric dipole moment $M_e = q_e l$, a dielectric particle can be regarded as an equivalent electric dipole with equivalent dipole moment $M_e^* = 2\pi\varepsilon_m(\varepsilon_p - \varepsilon_m)/(\varepsilon_p + \varepsilon_m) r^2 E_0$, where ε_m is the permittivity of the matrix; see Figure 1c.

Second, we consider the heat conduction equation $\nabla \cdot (-\kappa \nabla T) = \rho_h$ in two dimensions, where κ, T, and ρ_h are thermal conductivity, temperature, and thermal power density, respectively. Because of the similarity of equation forms, the thermal counterpart of an equivalent electric dipole is natural; say, $\kappa \to \varepsilon$, $\varphi \to T$, and $\rho_e \to \rho_h$. Therefore, with a uniform thermal field (K_0), a thermal particle (with thermal conductivity κ_p and radius r) can also exert the same effect as a thermal dipole (with hot source power q_h and distance l); see Figures 1d and 1e. We carefully discuss the equivalent thermal dipole in what follows.

The temperature distribution outside the thermal particle (T_m) in Figure 1d is [19]

$$T_m = -K_0 \rho \cos\theta + \frac{\kappa_p - \kappa_m}{\kappa_p + \kappa_m} r^2 K_0 \rho^{-1} \cos\theta + T_0, \quad (1)$$

where κ_m is the thermal conductivity of the matrix, and (ρ, θ) is the cylindrical coordinates. The second term on the right-hand side of equation (1) is caused by the thermal particle.

The temperature distribution (T) in Figure 1e is

$$T = -K_0 \rho \cos\theta + \frac{M_h}{2\pi\kappa_m} \rho^{-1} \cos\theta + T_0, \quad (2)$$

where the second term on the right-hand side is caused by the thermal dipole with dipole moment (M_h) defined as

$$M_h = q_h l. \quad (3)$$

We rewrite equation (1) according to the form of equation (2),

$$T_m = -K_0 \rho \cos\theta + \frac{M_h^*}{2\pi\kappa_m} \rho^{-1} \cos\theta + T_0, \quad (4)$$

where the second term on the right side can now be regarded as the effect caused by an equivalent thermal dipole with equivalent dipole moment (M_h^*) defined as

$$M_h^* = 2\pi\kappa_m \frac{\kappa_p - \kappa_m}{\kappa_p + \kappa_m} r^2 K_0. \quad (5)$$

Equation (5) establishes the relation between a thermal particle and a thermal dipole (Fig. 1f), which is similar to the relation between a dielectric particle and an electric dipole (Fig. 1c). In other words, a thermal particle can be regarded as an equivalent thermal dipole with equivalent dipole moment (M_h^*) determined by equation (5). Next, we discuss how to use the concept of equivalent thermal dipole to realize thermal illusion.

Thermal illusion is to design two different systems to possess the same thermal effect, and hence it can be used to mislead thermal detections. For example, if n_1 purple particles (with thermal conductivity κ_1 and radius r_1) plus n_2 brown particles (with thermal conductivity κ_2 and radius r_2) have the same thermal effect as n_3 red particles (with thermal conductivity κ_3 and radius r_3);

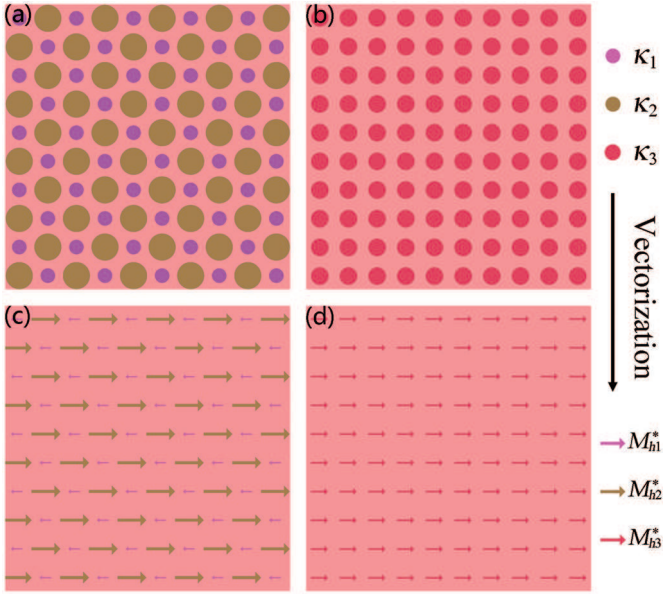

Fig. 2. Thermal illusion achieved by regarding thermal particles in (a, b) as equivalent thermal dipoles in (c, d). The physical explanation of vectorization is when the macroscopic equivalent thermal dipole moments of (c, d) are equal, thermal illusion between (a, b) can be realized.

see Figures 2a and 2b, the purpose of thermal illusion is achieved. A question is what requirement the two different systems should satisfy. It is difficult to directly answer this question because thermal conductivities do not possess additivity. To solve this problem, we should vectorize these thermal particles, and regard each one as an equivalent thermal dipole; see Figures 2c and 2d. Since the equivalent thermal dipole moments possess additivity, thermal illusion can be achieved when the macroscopic equivalent thermal dipole moments of two different systems are equal to each other,

$$n_1 M^*_{h1} + n_2 M^*_{h2} = n_3 M^*_{h3}, \tag{6}$$

where M^*_{hi} can be calculated by setting κ_p and r in equation (5) to be κ_i and r_i with $i = 1, 2, 3$.

Further, we discuss the material anisotropy [19] and geometry anisotropy [7] of a thermal particle, and build the relation between an anisotropic thermal particle and a thermal dipole, to ensure the research completeness.

If we consider the material anisotropy with thermal conductivity $\overleftrightarrow{\kappa}_p = \mathrm{diag}\,(\kappa_{\rho\rho}, \kappa_{\theta\theta})$, equation (5) can be extended to

$$M^*_h = 2\pi\kappa_m \frac{u\kappa_{\rho\rho} - \kappa_m}{u\kappa_{\rho\rho} + \kappa_m} r^2 K_0, \tag{7}$$

where $u = \sqrt{\kappa_{\theta\theta}/\kappa_{\rho\rho}}$, and $u\kappa_{\rho\rho}$ can be regarded as the effective scalar thermal conductivity (κ_p) corresponding to the tensorial one ($\overleftrightarrow{\kappa}_p$). Here, the anisotropic thermal conductivity is uniform in the cylindrical coordinates. For an anisotropic (even nonuniform) case in the Cartesian coordinates, an approximate method is to calculate the spatial average thermal conductivity along the direction of the external thermal field [15].

On the other hand, when we consider the geometry anisotropy of an ellipse particle (with vertical semiaxis s and horizontal semiaxis t), equation (5) can be extended to

$$M^*_h = \pi\kappa_m \frac{\kappa_p - \kappa_m}{\kappa_p L + \kappa_m (1 - L)} stK_0, \tag{8}$$

where the horizontal shape factor L is given by

$$L = \frac{st}{2} \int_0^\infty \frac{da}{(t^2 + a)\sqrt{(s^2 + a)(t^2 + a)}}. \tag{9}$$

Since the geometry is anisotropic, the effect of thermal illusion is also directional. Nevertheless, the analytical solution to a particle with both anisotropic material and geometry is difficult to derive, but we can resort to finite-element simulations to determine its effective thermal conductivity and thermal dipole moment.

Here, we only consider the thermal illusion between two types (purple and brown) of particles in Figure 2a and one (red) type of particles in Figure 2b. More generally, if we consider the thermal illusion between j types of particles (respectively with $n_1, n_2, \ldots, n_j$ particles) and $N - j$ types of particles (respectively with $n_{j+1}, n_{j+2}, \ldots, n_N$ particles), equation (6) can be extended to

$$\sum_{i=1}^{j} n_i M^*_{hi} = \sum_{i=j+1}^{N} n_i M^*_{hi}, \tag{10}$$

where M^*_{hi} can be calculated from equation (5), (7), or (8) with corresponding parameters.

Two comments on equation (10) are that (i) although the equivalent thermal dipole moment (M^*_{hi}) is dependent on the external field (K_0), equation (10) is independent of the external field (K_0) because each term contains a same K_0 which can be eliminated; and (ii) the equivalent thermal dipole moment (M^*_{hi}) is dependent on the matrix thermal conductivity. In other words, thermal illusion is independent of the external field (K_0), but dependent on the matrix thermal conductivity. The three-dimensional theory is presented in the Appendix.

So far, it is time to revisit the famous Bruggeman theory [35]. It is believed that the theory can explain the effective properties of the systems where the fractions of two materials are comparable. Also, the particles should be randomly distributed and may have overlaps [35,36]. However, "comparable", "randomly", and "overlaps" are three ambiguous descriptions. Here, we present a clear physical image to understand the Bruggeman theory. First, we write down the Bruggeman formula in two dimensions,

$$\phi \frac{\kappa_1 - \kappa_e}{\kappa_1 + \kappa_e} + (1 - \phi) \frac{\kappa_2 - \kappa_e}{\kappa_2 + \kappa_e} = 0, \tag{11}$$

where κ_e is the effective thermal conductivity of the two materials, and ϕ is the area fraction corresponding to the

material with thermal conductivity κ_1. We also rewrite our result [Eq. (6)] in a different way,

$$A_1\frac{\kappa_1-\kappa_m}{\kappa_1+\kappa_m}+A_2\frac{\kappa_2-\kappa_m}{\kappa_2+\kappa_m}=A_3\frac{\kappa_3-\kappa_m}{\kappa_3+\kappa_m}, \tag{12}$$

where $A_i=n_i\pi r_i^2$ with $i=1, 2, 3$. By taking $\kappa_3=\kappa_m=\kappa_e$ and $\phi=A_1/(A_1+A_2)$, our result [Eq. (12)] turns to the same form as the Bruggeman theory [Eq. (11)]. With the concept of equivalent thermal dipole and the understanding of equation (12) in this work, we find that the two terms on the left-hand side of equation (11) can be explained as the relative magnitudes of the macroscopic equivalent thermal dipole moments corresponding to the two materials. It is "relative magnitude" rather than "absolute magnitude" because $\phi=A_1/(A_1+A_2)$ and $1-\phi=A_2/(A_1+A_2)$ are area fractions. The summation of the two terms is zero, which means that the total dipole moment is zero and the two materials (with thermal conductivities κ_1 and κ_2) exert no influence on the matrix (with thermal conductivity κ_e). Thus, κ_e is defined as the effective thermal conductivity of the two materials. However, the difference is that here κ_e should be regarded as the thermal conductivity of a real matrix (a third material) where the original two materials are periodically embedded in the manner presented in Figure 2a. To sum up, the physical understanding of the Bruggeman theory [Eq. (11)] is that when it is satisfied, the two types of particles (with thermal conductivities κ_1 and κ_2) arranged in the manner presented in Figure 2a have the same property as the matrix (with thermal conductivity κ_e). This description is explicit without ambiguous words like "comparable", "randomly", and "overlaps". In other words, we provide a standard model (Fig. 2a) where the Bruggeman theory is clearly explained.

3 Finite-element simulations

We are now in a position to present two-dimensional finite-element simulations based on COMSOL Multiphysics[1] to confirm the proposed theory; see Figure 3. The thermal conductivities and particle sizes are designed according to equation (10).

We put two different types of particles (purple and brown) into the matrix (shown with 50% opaqueness in order not to cover the temperature distribution), and the isotherms are contracted; see Figure 3a. Then, we only put red particles into the matrix, and the isotherms are contracted with the same extent; see Figure 3b. Therefore, thermal illusion between purple plus brown particles in Figure 3a and red particles in Figure 3b is achieved. For quantitative analysis, Figure 3c shows the x component of the thermal field ($K_x=-\partial T/\partial x$) on the two solid black lines (one in x axis, the other in y axis) in each simulation box (Figs. 3a and 3b). In Figure 3c, black lines and red lines agree well with each other, but with some fluctuations in black lines.

It should be noted that such fluctuations result from the small particle numbers, rather than the imprecision of equation (10), because small particle numbers make the macroscopic equivalent thermal dipole moment locally nonuniform. To validate our explanation, we keep the thermal conductivities and area fractions of the three types of particles unchanged, and increase the particle numbers fourfold. The results are presented in Figures 3d–3f, and the fluctuations almost disappear as expected.

We further discuss thermal illusion between particles with material anisotropy; see Figures 3g–3i. The anisotropic thermal conductivity is expressed in cylindrical coordinates whose origin is at the center of each particle. In Figure 3i, the agreement between black lines and red lines validates the scheme with material anisotropy.

Finally, we discuss thermal illusion between more types of particles with geometry anisotropy; see Figures 3j–3l. There are four types of particles in Figure 3j. If we use the core-shell scheme, four times of calculations may be required to design four types of specific shells to realize thermal illusion. In this work, once calculation is enough; say, equation (10), because we consider the macroscopic effect of the four types of particles, rather than the local effect of a single type of particles. Therefore, our scheme is powerful to achieve thermal illusion in many-particle systems.

4 Laboratory experiments

According to the finite-element simulations in Figures 3j and 3k, we also conduct corresponding laboratory experiments; see Figure 4. The two samples are fabricated by drilling air holes on a copper plate with laser cut. Transparent plastic and foamed plastic (both insulated) are, respectively, applied on the upper and lower surfaces to reduce the infrared reflection and the thermal convection. By using the infrared camera FLIR E60, we measure the two samples between hot and cold baths; see Figures 4a and 4b. The corresponding measured results are presented in Figures 4c and 4d, which agree well with each other. Also, the experimental results (Figs. 4c and 4d) show good agreement with the finite-element simulations (Figs. 3j and 3k). So far, we may conclude that thermal illusion with the concept of equivalent thermal dipole has been validated by theory, finite-element simulations, and laboratory experiments.

5 Discussion and conclusion

In the theoretical derivation to achieve thermal illusion, we have ignored an inessential detail; say, the dipole-dipole interaction. When writing down equation (1), we have supposed that the matrix size is far larger than the particle size. However, when thermal particles (or equivalent thermal dipoles) are big and become close to each other, the dipole-dipole interaction will exert some influence on equation (1). Fortunately, the periodic arrangement ensures the certain distance between particles, and thus the local fluctuations of particle distances are minimized to the lowest extent [37].

[1] http://www.comsol.com/

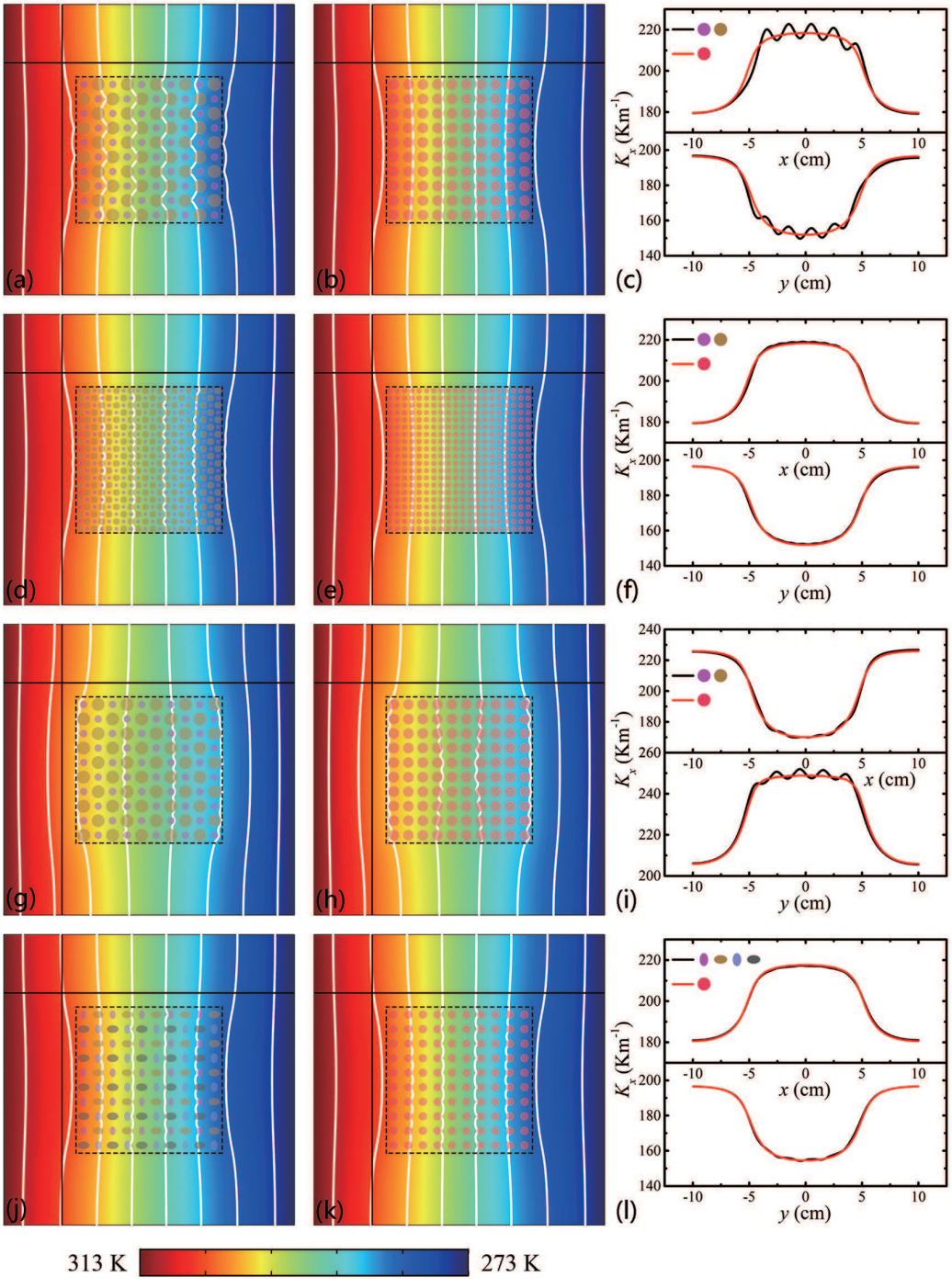

Fig. 3. Finite-element simulations of thermal illusion with (a–c, d–f) isotropic particles, (g–i) material anisotropic particles, and (j–l) geometry-anisotropic particles. The simulation box is 20×20 cm^2, and the dashed square is 10×10 cm^2. The two solid black lines are located at $x = -6$ and $y = 6$ cm, and the origin is at the center of each simulation box. The temperature of the left (or right) boundary is set at 313 K (or 273 K), and the other boundaries are insulated. The thermal conductivities and particles sizes are all designed according to equation (10). The thermal conductivities of the matrices in (a, b, d, e), (g, h), and (j, k) are 200, 20, 400 Wm^{-1} K^{-1}, respectively. The particle distances in (a, b, g, h, j, k) and (d, e) are 10 and 5 mm, respectively. Other parameters are as follows. (a) 50 purple particles with $\kappa_1 = 400$ Wm^{-1} K^{-1}, $r_1 = 2.52$ mm; 50 brown particles with $\kappa_2 = 1$ Wm^{-1} K^{-1}, $r_2 = 4.37$ mm. (b) 100 red particles with $\kappa_3 = 41$ Wm^{-1} K^{-1}, $r_3 = 3.57$ mm. (d) 200 purple particles with $\kappa_1 = 400$ Wm^{-1} K^{-1}, $r_1 = 1.26$ mm; 200 brown particles with $\kappa_2 = 1$ Wm^{-1} K^{-1}, $r_2 = 2.19$ mm. (e) 400 red particles with $\kappa_3 = 41$ Wm^{-1} K^{-1}, $r_3 = 1.78$ mm. (g) 50 purple particles with diag (400, 225) Wm^{-1} K^{-1}, $r_1 = 2.52$ mm; 50 brown particles with diag (200, 50) Wm^{-1} K^{-1}, $r_2 = 4.37$ mm. (h) 100 red particles with diag (244, 61) Wm^{-1} K^{-1}, $r_3 = 3.57$ mm. (j) 25 purple particles with $\kappa_1 = 0.025$ Wm^{-1} K^{-1}, $s_1 = 2.93$ mm, $t_1 = 1.95$ mm; 25 brown particles with $\kappa_2 = 0.025$ Wm^{-1} K^{-1}, $s_2 = 2.44$ mm, $t_2 = 3.66$ mm; 25 blue particles with $\kappa_3 = 0.025$ Wm^{-1} K^{-1}, $s_3 = 3.24$ mm, $t_3 = 2.16$ mm; 25 dark particles with $\kappa_4 = 0.025$ Wm^{-1} K^{-1}, $s_4 = 2.61$ mm, $t_4 = 3.91$ mm. (k) 100 red particles with $\kappa_5 = 0.025$ Wm^{-1} K^{-1}, $r_5 = 2.82$ mm.

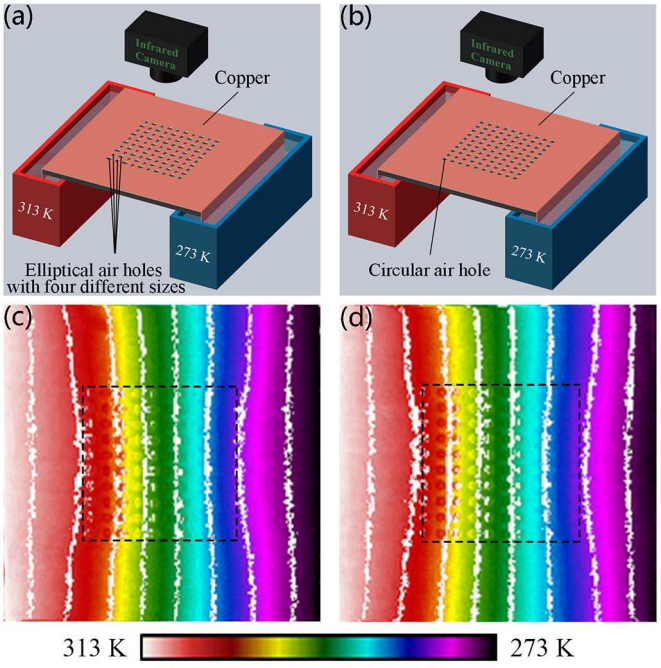

Fig. 4. Laboratory experiments for confirming the finite-element simulations shown in Figures 3j and 3k. (a, b) are the schematic diagrams showing two fabricated samples and the experimental devices. The thermal conductivities and the sizes are the same as those for Figures 3j and 3k, respectively. (c, d) display the experimental measurement results of the sample shown in (a, b), respectively. Parameters: copper's thermal conductivity 400 $\mathrm{Wm^{-1}\,K^{-1}}$ and air's thermal conductivity 0.025 $\mathrm{Wm^{-1}\,K^{-1}}$.

Nevertheless, here we only discuss the simplest square lattice. It is just a beginning, and more complex lattices remain to be studied, which may contain more interesting points. For example, the rectangle lattice is characterized by the lattice anisotropy, which may result in the different macroscopic equivalent thermal dipole moment compared with the square lattice. Certainly, the transient results can also be expected, if we consider the density and heat capacity appropriately [24].

In summary, we have established the relation between a thermal particle and a thermal dipole, and realized thermal illusion with the concept of equivalent thermal dipole, namely setting the macroscopic equivalent thermal dipole moments of two different systems to be the same. We also demonstrate a clear physical image to understand the famous Bruggeman theory. Theoretical analysis is further validated by finite-element simulations and laboratory experiments. Our mechanism is efficient to handle many-particle problems, and has potential applications in misleading infrared detection, manipulating heat flux, etc. The related conclusions can also be directly extended to other diffusion fields, such as those in magnetostatics [38–40] and electrostatics [41].

We acknowledge the financial support by the National Natural Science Foundation of China under Grant No. 11725521.

Author contribution statement

All the authors were involved in the preparation of the manuscript. All the authors have read and approved the final manuscript. L.X. and J.H. designed research; L.X. and S.Y. performed research and analyzed data; and L.X., S.Y., and J.H. wrote the paper.

Appendix A: Theory for three dimensions

The key to three-dimensional thermal illusion is to establish the relation between a three-dimensional thermal particle and a three-dimensional thermal dipole. For this purpose, we should extend equations (5), (7), and (8) to three dimensions. The three-dimensional counterparts of equations (1) and (2) are, respectively,

$$T_m = -K_0\rho\cos\theta + \frac{\kappa_p-\kappa_m}{\kappa_p+2\kappa_m}r^3K_0\rho^{-2}\cos\theta + T_0, \quad \text{(A.1)}$$

$$T = -K_0\rho\cos\theta + \frac{M_h}{4\pi\kappa_m}\rho^{-2}\cos\theta + T_0, \quad \text{(A.2)}$$

where the three-dimensional thermal dipole moment M_h can also be described by equation (3).

We rewrite equation (A.1) according to the form of equation (A.2),

$$T_m = -K_0\rho\cos\theta + \frac{M_h^*}{4\pi\kappa_m}\rho^{-2}\cos\theta + T_0, \quad \text{(A.3)}$$

where the equivalent thermal dipole moment (M_h^*) in three dimensions can be defined as

$$M_h^* = 4\pi\kappa_m\frac{\kappa_p-\kappa_m}{\kappa_p+2\kappa_m}r^3K_0. \quad \text{(A.4)}$$

Equation (A.4) is the three-dimensional counterpart of equation (5).

When considering three-dimensional material anisotropy with thermal conductivity $\overleftrightarrow{\kappa}_p = \mathrm{diag}\,(\kappa_{\rho\rho}, \kappa_{\theta\theta}, \kappa_{\varphi\varphi})$ with $\kappa_{\theta\theta} = \kappa_{\varphi\varphi}$ in spherical coordinates (ρ, θ, φ), equation (A.4) can be extended to

$$M_h^* = 4\pi\kappa_m\frac{\upsilon\kappa_{\rho\rho}-\kappa_m}{\upsilon\kappa_{\rho\rho}+2\kappa_m}r^3K_0, \quad \text{(A.5)}$$

where $\upsilon = -1/2 + \sqrt{1/4 + 2\kappa_{\theta\theta}/\kappa_{\rho\rho}}$. Equation (A.5) is the three-dimensional counterpart of equation (7).

On the other hand, when considering three-dimensional geometry anisotropy of an ellipsoid particle (with the third semiaxis w), equation (A.4) becomes

$$M_h^* = \frac{4}{3}\pi\kappa_m\frac{\kappa_p-\kappa_m}{\kappa_pL+\kappa_m\,(1-L)}stwK_0, \quad \text{(A.6)}$$

where the horizontal shape factor L is given by

$$L = \frac{stw}{2} \int_0^\infty \frac{da}{(t^2+a)\sqrt{(s^2+a)(t^2+a)(w^2+a)}}. \tag{A.7}$$

Equations (A.6) and (A.7) are the three-dimensional counterpart of equations (8) and (9), respectively.

Then, thermal illusion can be achieved when the three-dimensional macroscopic equivalent thermal dipole moments of j types of particles (with n_1, n_2, ..., n_j particles, respectively) and $N-j$ types of particles (with n_{j+1}, n_{j+2}, ..., n_N particles, respectively) are equal,

$$\sum_{i=1}^{j} n_i M_{hi}^* = \sum_{i=j+1}^{N} n_i M_{hi}^*, \tag{A.8}$$

where M_{hi}^* can be calculated from equation (A.4), (A.5), or (A.6) with corresponding parameters. Equation (A.8) is the three-dimensional counterpart of equation (10). In fact, the mathematical forms of equation (A.8) and equation (10) are totally the same, only with different calculation of M_{hi}^*.

References

1. C.Z. Fan, Y. Gao, J.P. Huang, Appl. Phys. Lett. **92**, 251907 (2008)
2. T.Y. Chen, C.N. Weng, J.S. Chen, Appl. Phys. Lett. **93**, 114103 (2008)
3. S. Narayana, Y. Sato, Phys. Rev. Lett. **108**, 214303 (2012)
4. H.Y. Xu, X.H. Shi, F. Gao, H.D. Sun, B.L. Zhang, Phys. Rev. Lett. **112**, 054301 (2014)
5. T.C. Han, X. Bai, D.L. Gao, J.T.L. Thong, B.W. Li, C.W. Qiu, Phys. Rev. Lett. **112**, 054302 (2014)
6. Y.G. Ma, Y.C. Liu, M. Raza, Y.D. Wang, S.L. He, Phys. Rev. Lett. **113**, 205501 (2014)
7. T.C. Han, P. Yang, Y. Li, D.Y. Lei, B.W. Li, K. Hippalgaonkar, C.W. Qiu, Adv. Mater. **30**, 1804019 (2018)
8. Y. Li, K.J. Zhu, Y.G. Peng, W. Li, T.Z. Yang, H.X. Xu, H. Chen, X.F. Zhu, S.H. Fan, C.W. Qiu, Nat. Mater. **18**, 48 (2018)
9. L.J. Xu, J.P. Huang, Phys. Rev. Appl. **12**, 044048 (2019)
10. T.C. Han, J.J. Zhao, T. Yuan, D.Y. Lei, B.W. Li, C.W. Qiu, Energy Environ. Sci. **6**, 3537 (2013)
11. R.S. Kapadia, P.R. Bandaru, Appl. Phys. Lett. **105**, 233903 (2014)
12. T.Y. Chen, C.N. Weng, Y.L. Tsai, J. Appl. Phys. **117**, 054904 (2015)
13. G.Q. Xu, H.C. Zhang, Q. Zou, Y. Jin, M. Xie, Int. J. Heat Mass Transfer **115**, 682 (2017)
14. G.Q. Xu, H.C. Zhang, Y. Jin, S. Li, Y. Li, Opt. Express **25**, A419 (2017)
15. L.J. Xu, S. Yang, J.P. Huang, Phys. Rev. E **98**, 052128 (2018)
16. K.P. Vemuri, P.R. Bandaru, Appl. Phys. Lett. **104**, 083901 (2014)
17. T.Z. Yang, K.P. Vemuri, P.R. Bandaru, Appl. Phys. Lett. **105**, 083908 (2014)
18. K.P. Vemuri, F.M. Canbazoglu, P.R. Bandaru, Appl. Phys. Lett. **105**, 193904 (2014)
19. L.J. Xu, S. Yang, J.P. Huang, Phys. Rev. E **99**, 022107 (2019)
20. L.J. Xu, S. Yang, J.P. Huang, Phys. Rev. Appl. **11**, 054071 (2019)
21. T.C. Han, X. Bai, J.T.L. Thong, B.W. Li, C.W. Qiu, Adv. Mater. **26**, 1731 (2014)
22. X. He, L.Z. Wu, Appl. Phys. Lett. **105**, 221904 (2014)
23. T.Z. Yang, X. Bai, D.L. Gao, L.Z. Wu, B.W. Li, J.T.L. Thong, C.W. Qiu, Adv. Mater. **27**, 7752 (2015)
24. T.Z. Yang, Y. Su, W. Xu, X.D. Yang, Appl. Phys. Lett. **109**, 121905 (2016)
25. Y. Li, X. Bai, T.Z. Yang, H. Luo, C.W. Qiu, Nat. Commun. **9**, 273 (2018)
26. R. Hu, S.L. Zhou, Y. Li, D.Y. Lei, X.B. Luo, C.W. Qiu, Adv. Mater. **30**, 1707237 (2018)
27. S.L. Zhou, R. Hu, X.B. Luo, Int. J. Heat Mass Transfer **127**, 607 (2018)
28. L.J. Xu, C.R. Jiang, J.P. Huang, Eur. Phys. J. B **91**, 166 (2018)
29. S.Y. Lu, H.C. Lin, J. Appl. Phys. **79**, 6761 (1996)
30. S.Y. Lu, J. Appl. Phys. **84**, 2647 (1998)
31. S.Y. Lu, J. Appl. Phys. **85**, 264 (1999)
32. X.F. Zhou, L. Gao, J. Appl. Phys. **103**, 083503 (2008)
33. H.L. Fu, L. Gao, Phys. Lett. A **375**, 3588 (2011)
34. H.L. Fu, L. Gao, Int. J. Therm. Sci. **61**, 61 (2012)
35. D.A.G. Bruggeman, Ann. Phys. **24**, 636 (1935)
36. M. Wang, N. Pan, Mater. Sci. Eng. R **63**, 1 (2008)
37. L.J. Xu, S. Yang, J.P. Huang, Phys. Rev. Appl. **11**, 034056 (2019)
38. R.M. Batlle, A. Parra, S. Laut, N.D. Valle, C. Navau, A. Sanchez, Phys. Rev. Appl. **9**, 034007 (2018)
39. W. Jiang, Y.G. Ma, S.L. He, Phys. Rev. Appl. **9**, 054041 (2018)
40. L.J. Xu, J.P. Huang, Europhys. Lett. **125**, 64001 (2019)
41. L.J. Xu, J.P. Huang, Eur. Phys. J. B **92**, 53 (2019)